Theory of the coplanar-waveguide Penning trap

Article (Published Version)

Theory of the coplanar-waveguide Penning trap

2011 New J. Phys. 13 113029

(http://iopscience.iop.org/1367-2630/13/11/113029)

New Journal of Physics
The open-access journal for physics

Theory of the coplanar-waveguide Penning trap

J Verdú

Department of Physics and Astronomy, University of Sussex,
Falmer BN1 9QH, UK
E-mail: J.L.Verdu-Galiana@sussex.ac.uk

New Journal of Physics **13** (2011) 113029 (18pp)
Received 8 February 2011
Published 18 November 2011
Online at http://www.njp.org/
doi:10.1088/1367-2630/13/11/113029

Abstract. A novel planar Penning trap is presented, which results from the projection of the well-known three-dimensional cylindrical trap onto the surface of a chip. The introduced trap is also a coplanar-waveguide cavity, similar to those used in circuit quantum electrodynamics experiments with superconducting two-level systems. It opens up the possibility of integrating a single trapped electron, or geonium atom, into quantum circuits. The trap is an elliptical Penning trap, with the magnetic field parallel to the chip's surface. A design procedure is described, which permits the compensation of electric anharmonicities up to sixth order. This should render possible the observation of a single trapped electron and the accurate measurement of its eigenfrequencies, a *sine qua non* requirement for a useful planar geonium technology.

Contents

1. Introduction

A single electron in a Penning trap is known as a geonium atom [1], as coined by its inventor, the 1989 Nobel Prize winner H Dehmelt. It is an outstanding system for measuring fundamental constants and testing the laws of physics [2]. Examples include measurement of the electron's g-factor [3] and mass [4]. Electrons in cryogenic Penning traps have been proposed for implementing a quantum processor [5–7]. Initially motivated by the scalability requirements for quantum computation [8], a planar Penning trap has been conceived at the University of Mainz [9]. Trapping of electrons has been demonstrated with it, both at room temperature and with a cryogenic setup [10, 11]. Recently, several optimized versions of the Mainz trap have been proposed at Harvard [12]. These should pave the way for the observation of a single electron, a primary goal not yet achieved with planar Penning traps [11].

In this paper, the coplanar-waveguide (CPW) Penning trap has been introduced. Its design is inspired by modern planar microwave technology. Superconducting MW-cavities have been built on a chip with very low losses, achieving quality factors in the range of $Q \sim 10^5$–10^6 [13]. The basis of those cavities is the CPW-transmission line, consisting of a central conducting strip and two outer ground-planes [14]. The mentioned high-Q resonators have triggered the field of circuit-quantum electrodynamics (circuit-QED) [15, 16]. As explained in the following sections, the CPW-Penning trap originates from the projection of the well-known cylindrical trap [17] onto the surface of a chip. That projection naturally results in a finite section of the CPW-transmission line. This can function as a cavity or, alternatively, can be coupled to the mentioned circuit-QED resonators. Hence, the CPW-trap opens up the possibility of a

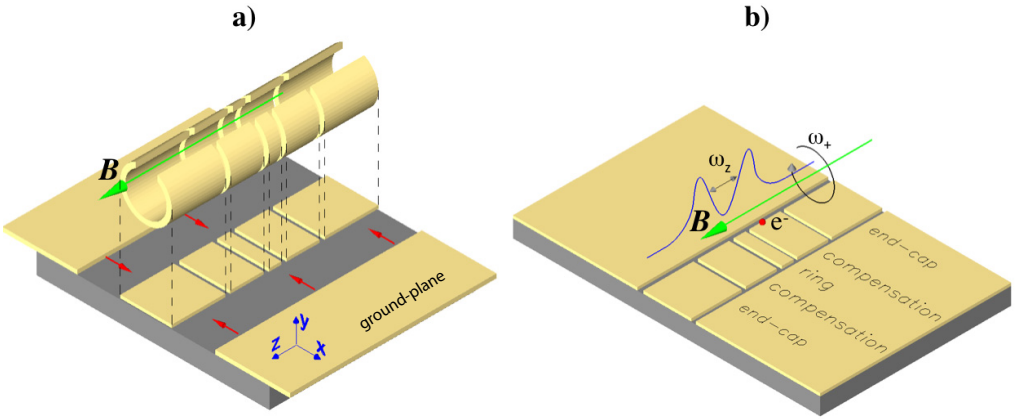

Figure 1. (a) Genesis of the CPW-Penning trap. The figure shows the projection of a standard cylindrical five-pole Penning trap onto a plane. The projected segments are shielded with two outer ground-planes. (b) Sketch of the CPW-trap, with the resulting cyclotron and axial motions of an electron (see section 2.3).

geonium atom becoming a building block of future 'quantum circuits'. Electrons have already demonstrated practical applications in circuit-QED. An example is the recently achieved high-cooperativity coupling of electron-spin ensembles—housed in ruby and diamond coatings in the chip—to superconducting CPW-cavities [18]. The aim is to provide those circuits with long-coherence quantum memories. Other systems have also been considered for the storage of quantum information and other circuit-QED applications, such as Bose–Einstein condensates [19] and polar molecules [20]. A detailed discussion of the possibilities of a geonium atom in superconducting quantum circuits goes beyond the scope of this paper; that will be treated in future publications.

2. Coplanar-waveguide (CPW) Penning trap

The genesis of the CPW-Penning trap can be described in the following way. Starting from a hypothetical cylindrical trap [17], an imaginary cut is performed along its surface, as shown in figure 1(a). The imaginary slit permits one to virtually 'stress' and 'flatten' the originally cylindrical electrodes. These are transformed into flat rectangular segments and then projected onto a plane. At both sides of the projected segments, two outer ground-planes are added, for shielding and equipotential reference. The magnetic field of the original three-dimentional (3D) trap, $\vec{B} = B \cdot \hat{u}_z$, is left unchanged and is parallel to the surface of the chip. The obtained set of electrodes together with the ground planes, form a section of a CPW-transmission line, such as those used in circuit-QED [15, 16]. The denomination *CPW-Penning trap* is chosen for this reason.

As sketched in figure 1(b), the basic CPW-Penning trap consists of five planar electrodes: the 'ring', two compensation electrodes and two end-caps.

2.1. Electrostatic trapping potential

For simplicity, we assume that the conducting chip housing the trap extends to infinity. With it, the calculation of the trapping potential is straightforward; details are explained in appendix A.

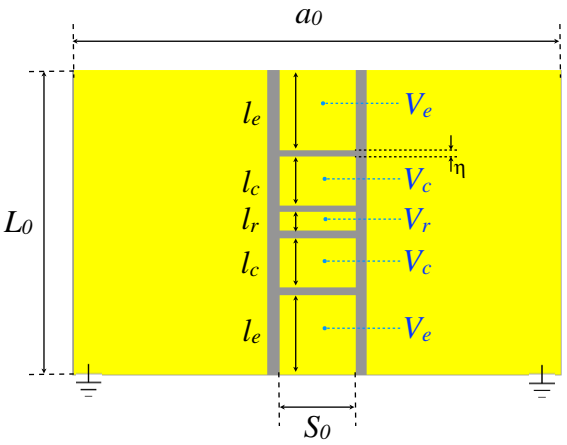

Figure 2. Dimensions of the CPW-trap and applied voltages. The origin of the coordinate system, (0, 0, 0), is located at the centre of the ring electrode.

The result is

$$\phi(x, y, z) = V_\mathrm{r} \cdot f_\mathrm{r}(x, y, z) + V_\mathrm{c} \cdot f_\mathrm{c}(x, y, z) + V_\mathrm{e} \cdot f_\mathrm{e}(x, y, z) + f_\mathrm{gaps}(x, y, z \mid V_\mathrm{r}, V_\mathrm{c}, V_\mathrm{e}). \quad (1)$$

The symbols V_r, V_c and V_e represent the applied dc-voltages to the ring, compensation electrodes and end-caps, respectively. This is sketched in figure 2. The functions f_r, f_c and f_e depend only on the dimensions of the trap (see equation (A.2)). On the contrary, f_gaps, which represents the contribution to the potential of all insulating gaps, depends on both the geometry and all the applied voltages (see equation (A.2)).

2.1.1. Example of a CPW-Penning trap. The basic functioning of a CPW-trap is best illustrated by computing an example with equation (1). For this purpose, we choose $l_\mathrm{r} = 0.9$, $l_\mathrm{c} = 2.0$, $l_\mathrm{e} = 5.0$, $\eta = 0.1$ and $S_0 = 7.0$ (all in mm). The choice of this geometry is in principle arbitrary; however, this concrete example will serve, throughout this paper, to elucidate the main properties of the CPW-trap. The discussion will also be focused on a single electron at cryogenic temperatures.

For the example of figure 3, the voltages are (all in Volt) $V_\mathrm{r} = -1$, $V_\mathrm{c} = -1.15$ and $V_\mathrm{e} = -4$. These allow capture of electrons or any negatively charged particles around the position $(x = 0, y = y_0, z = 0)$. In contrast to the cylindrical trap, the end-caps cannot be grounded; actually, $|V_\mathrm{e}| > |V_\mathrm{c}| \gtrapprox |V_\mathrm{r}|$ must hold. This is required for the existence of an equilibrium position at some $y_0 > 0$ above the chip's surface. The continuous smooth curve in figure 3(a) shows the actual shape of the electric potential at y_0 ($\simeq 1.37$ mm, for the example). The variation of ϕ along the vertical axes y is shown in figure 3(b).

2.1.2. Equilibrium position of the trap. y_0 is determined by the equality $\frac{\partial\phi(0,y,0)}{\partial y}|_{y=y_0} = 0$. If the insulating gaps are vanishingly small, $\eta \to 0$, then $f_\mathrm{gaps} \to 0$ (see equation (A.2)). With this approximation, the equation for calculating y_0 is

$$\left.\frac{\partial f_\mathrm{r}}{\partial y}\right|_{y=y_0} + T_\mathrm{c} \cdot \left.\frac{\partial f_\mathrm{c}}{\partial y}\right|_{y=y_0} + T_\mathrm{e} \cdot \left.\frac{\partial f_\mathrm{r}}{\partial y}\right|_{y=y_0} = 0. \quad (2)$$

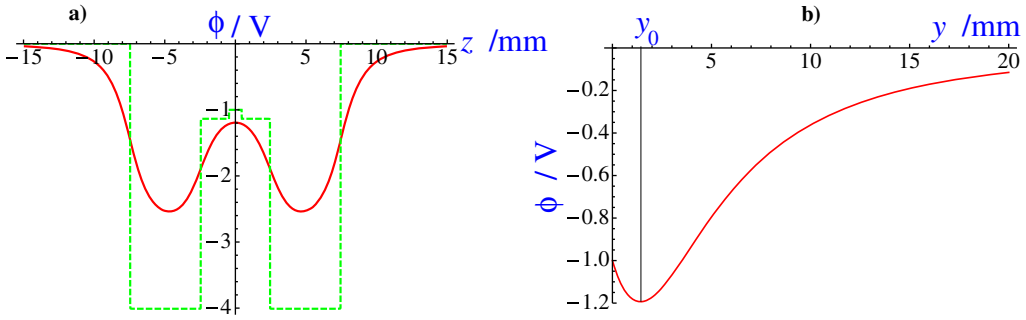

Figure 3. Example of the electrostatic potential of a CPW-cavity Penning trap. The graphs are calculated with $\phi(x, y, z)$ of equation (1). The dashed curve in (a) shows the applied voltages at the trap's electrodes.

We have introduced the *tuning ratio* $T_c = \frac{V_c}{V_r}$ and the *end-cap to ring ratio* $T_e = \frac{V_e}{V_r}$. Equation (2) shows that the trapping height depends only on voltage ratios T_c, $T_e \rightarrow y_0 = y_0(T_c, T_e)$. This formal dependence also holds for the less restrictive case that η is small 'enough', $\eta \ll l_r, l_c, l_e, S_0$ (see the discussion in appendix A). Equation (2) cannot be solved analytically for y_0; only numerical values can be obtained.

2.2. *Expansion of the potential around the equilibrium position*

The series expansion of $\phi(x, y, z)$ around the equilibrium position $(0, y_0, 0)$, including terms up to the fourth order, has the following form:

$$\begin{aligned}\phi(x, y, z) = \phi(0, y_0, 0) + \cdots + \underbrace{C_{002}\, z^2 + C_{200}\, x^2 + C_{020}\,(y - y_0)^2}_{\phi_{\text{quad}}} \\ + \underbrace{C_{012}\, z^2 (y - y_0) + C_{210}\, x^2\,(y - y_0) + C_{030}\,(y - y_0)^3}_{\text{odd anharmonicities}} \\ + \underbrace{C_{202}\, z^2\, x^2 + C_{022}\, z^2\,(y - y_0)^2 + C_{220}\, x^2\,(y - y_0)^2 + C_{004}\, z^4 + C_{400}\, x^4 + C_{040}\,(y - y_0)^4}_{\text{even anharmonicities}}.\end{aligned} \tag{3}$$

The expansion coefficients are defined by $C_{ijk} = \frac{1}{i!\,j!\,k!} \cdot \frac{\partial^{i+j+k}\,\phi(x,y,z)}{\partial x^i\,\partial y^j\,\partial z^k}\big|_{(0,y_0,0)}$. The symmetry of $\phi(x, y, z)$ along $\hat{u}_x$ and $\hat{u}_z$ implies that all C_{ijk} with odd i and/or odd k vanish. The C_{ijk}-coefficients define to a great extent the performance of the trap. They (or equivalent ones) have been studied in detail for cylindrical [17], hyperbolic [21] and toroidal Penning traps [22]. Moreover, as for equation (2), if the slits between electrodes are small 'enough', then C_{ijk} scale linearly with the ring voltage $\Rightarrow C_{ijk} = V_r \cdot c_{ijk}$, where $c_{ijk} = c_{ijk}(T_c, T_e)$ depend only on T_c and T_e.

2.2.1. Constraints on the C_{ijk}-coefficients. Plugging the series expansion (3) into the Laplace equation, $\nabla^2\phi(x, y, z) = 0$, the following equalities can be obtained:

$$C_{200} + C_{020} + C_{002} = 0; \quad 3\,C_{030} + C_{210} + C_{012} = 0. \tag{4}$$

$$6\,C_{400} + C_{220} + C_{202} = 0; \quad 6\,C_{040} + C_{220} + C_{022} = 0; \quad 6\,C_{004} + C_{202} + C_{022} = 0. \tag{5}$$

In the case of a 3D hyperbolic or cylindrical trap, the coordinates x and y are undistinguishable $\Rightarrow C_{200} = C_{020}$. Thus, equation (4) (left) reduces to $C_{200} = -2\,C_{020}$. From it, the potential of an ideal classical Penning trap arises $\Rightarrow \phi = C_{002}(z^2 - (x^2+y^2)/2)$. In the case of the CPW-trap, though, x and y are distinguishable and the curvatures C_{200} and C_{020} are not identical: $C_{200} \neq C_{020}$. Hence, the general form of the pure quadrupole potential, i.e. including terms only up to second order, is

$$\phi_{\text{quad}}(x, y, z) = C_{002} \cdot \left(z^2 - \frac{x^2 + (y - y_0)^2}{2} \right) + \frac{1}{2}\, C_{002}\, \epsilon \cdot (x^2 - (y - y_0)^2). \qquad (6)$$

The *ellipticity parameter* is given by $\epsilon = \frac{C_{200} - C_{020}}{C_{002}}$. In general, $\epsilon \neq 0$, and the CPW-trap is therefore an elliptical Penning trap [23, 24].

2.3. Ideal elliptical CPW-Penning trap

The motion of a particle in the ideal elliptical trap of equation (6) has been calculated by Kretzschmar [24]. The reduced cyclotron ($\omega_{\text{p}} = 2\pi\,\nu_{\text{p}}$), magnetron ($\omega_{\text{m}} = 2\pi\,\nu_{\text{m}}$) and axial ($\omega_z = 2\pi\,\nu_z$) frequencies of the trapped particle—with charge q and mass m—are

$$\omega_{\text{p}} = \sqrt{\tfrac{1}{2}(\omega_{\text{c}}^2 - \omega_z^2) + \tfrac{1}{2}\sqrt{\omega_{\text{c}}^2\,\omega_1^2 + \epsilon^2\,\omega_z^4}}; \quad \omega_{\text{m}} = \sqrt{\tfrac{1}{2}(\omega_{\text{c}}^2 - \omega_z^2) - \tfrac{1}{2}\sqrt{\omega_{\text{c}}^2\,\omega_1^2 + \epsilon^2\,\omega_z^4}};$$

$$\omega_z = \sqrt{2\,C_{002}\,\frac{q}{m}} \quad \text{with} \quad \omega_{\text{c}} = \frac{q}{m} \cdot B \quad \text{and} \quad \omega_1 = \sqrt{\omega_{\text{c}}^2 - 2\,\omega_z^2}. \qquad (7)$$

When $\epsilon = 0$, the usual expressions [25] for the frequencies of a 'circular' Penning trap are recovered. For the example of figure 3, the ellipticity is $\epsilon \simeq 0.41$. According to equation (7), the frequencies of a trapped electron are $\omega_{\text{p}} = 2\pi \cdot 14\,\text{GHz}$, $\omega_z = 2\pi \cdot 28\,\text{MHz}$ and $\omega_{\text{m}} = 2\pi \cdot 26\,\text{kHz}$. A magnetic field of $B = 0.5\,\text{T}$ is assumed, motivated by the suitability of the corresponding cyclotron frequency for circuit-QED applications [15].

The radial motion in an ideal elliptical trap is $(x(t), y(t) - y_0) = (A_{\text{p}}\,\xi_{\text{p}}\cos(\omega_{\text{p}}t) + A_{\text{m}}\,\xi_{\text{m}}\cos(\omega_{\text{m}}t),\, A_{\text{p}}\eta_{\text{p}}\sin(\omega_{\text{p}}t) + A_{\text{m}}\eta_{\text{m}}\sin(\omega_{\text{m}}t))$, where the amplitudes are given by

$$A_{\text{p}} = \frac{1}{\omega_{\text{p}}}\sqrt{\frac{2E_{\text{p}}}{\gamma_{\text{p}}\,m}}, \quad \gamma_{\text{p}} = 1 - \frac{\omega_z^2}{2\,\omega_{\text{p}}^2} \simeq 1; \quad A_{\text{m}} = \sqrt{\frac{2\,E_{\text{m}}}{(\omega_{\text{m}}^2 - \omega_z^2/2)\,m}}, \qquad (8)$$

and [24]

$$\xi_{\text{p,m}} = \sqrt{\frac{\omega_{\text{c}}^2 + \epsilon\,\omega_z^2 \pm \sqrt{\omega_{\text{c}}^2\,\omega_1^2 + \epsilon^2\,\omega_z^4}}{2\omega_{\text{p}}/\omega_1\sqrt{\omega_{\text{c}}^2\,\omega_1^2 + \epsilon^2\,\omega_z^4}}}; \quad \eta_{\text{p,m}} = \sqrt{\frac{\omega_{\text{c}}^2 - \epsilon\,\omega_z^2 \pm \sqrt{\omega_{\text{c}}^2\,\omega_1^2 + \epsilon^2\,\omega_z^4}}{2\omega_{\text{p}}/\omega_1\sqrt{\omega_{\text{c}}^2\,\omega_1^2 + \epsilon^2\,\omega_z^4}}}. \qquad (9)$$

The symbols E_{p} and E_{m} represent the cyclotron and magnetron energies, respectively. As shown by Kretzschmar, the orbit of the reduced cyclotron motion is only slightly affected by the ellipticity: $\xi_{\text{p}} \simeq \eta_{\text{p}} \simeq 1$. It very nearly follows the circular shape of conventional Penning traps. In contrast, the magnetron motion becomes an ellipse, where the orientation of the major and minor axes (along x or y) depends on the sign of ϵ. Moreover, that motion is stable for $-1 < \epsilon < 1$ and, at the limit $|\epsilon| \to 1$, it becomes very slow, $\omega_{\text{m}} \to 0$. In that case, the magnetron ellipse tends towards a line, with an increasingly wide major axes and a vanishing minor one (if $\epsilon \to +1 \Rightarrow \xi_{\text{m}} \to \infty$, $\eta_{\text{m}} \to 0$ and vice versa). For values $|\epsilon| \geqslant 1$, the magnetron becomes an unbounded hyperbolic motion and trapping is not possible [24].

3. Electrical anharmonicities

The ideal trap described in section 2.3 is only valid for vanishing amplitudes of the particle's motion. In real experiments the electric anharmonicities must be taken into account. These generate energy-dependent fluctuations/deviations of the particle's frequencies.

3.1. Frequency-shifts matrix

All anharmonicities, even and odd, up to the fourth order in the expansion of ϕ, $3 \leqslant i+j+k \leqslant 4$ (see equation (3)), produce frequency shifts that scale linearly with the energies of the particle. Hence, they can be expressed in matrix form:

$$\begin{pmatrix} \Delta\nu_{\mathrm{p}} \\ \Delta\nu_z \\ \Delta\nu_{\mathrm{m}} \end{pmatrix} = \underbrace{\begin{pmatrix} M_{1,1} & M_{1,2} & M_{1,3} \\ M_{2,1} & M_{2,2} & M_{2,3} \\ M_{3,1} & M_{3,2} & M_{3,3} \end{pmatrix}}_{M\,=\,\text{frequency-shifts matrix}} \begin{pmatrix} \Delta E_{\mathrm{p}} \\ \Delta E_z \\ \Delta E_{\mathrm{m}} \end{pmatrix}. \tag{10}$$

Each perturbation to ϕ_{quad} appearing in equation (3) delivers such a *frequency-shifts matrix*. In total, the CPW-cavity trap requires nine M^{ijk} matrices, corresponding to each C_{ijk} perturbative Hamiltonian. The expressions for all M^{ijk} are given in appendix B. The overall frequency-shifts matrix is the sum of all of them:

$$M = M^{012} + M^{210} + M^{030} + M^{220} + M^{202} + M^{022} + M^{004} + M^{400} + M^{040}. \tag{11}$$

For a single electron captured in the example trap of section 2.1.1, with the voltages of figure 3 and $B = 0.5\,\mathrm{T}$, the overall frequency-shifts matrix is

$$M = \begin{pmatrix} 5\times10^{-6} & 0.5 & -0.9 \\ 1\times10^{-3} & 203 & -411 \\ -2\times10^{-6} & -0.4 & 2 \end{pmatrix} \mathrm{Hz\,K^{-1}}. \tag{12}$$

3.2. Compensation of $\frac{\Delta\nu_z}{\Delta E_z}$: optimal tuning ratio

The accurate measurement of the axial frequency is essential; in most cases the determination of the other electron's eigenfrequencies or spin state depends upon it [2, 26]. Thus, $M_{2,2} = \frac{\Delta\nu_z}{\Delta E_z}$ is the most relevant and dangerous of all frequency shifts in M. In the example, it amounts to $203\,\mathrm{Hz\,K^{-1}}$. Such a dependence of ν_z on the axial energy—which is not constant but fluctuating [27]—would render the detection of the electron almost impossible, even at cryogenic temperatures.

According to (B.1) and (B.7), $M_{2,2}$ is given by the sum of $M^{004}_{2,2}$ and $M^{012}_{2,2}$. Taking into account that $\nu_{\mathrm{m}} \ll \nu_z \ll \nu_{\mathrm{p}}$, we have

$$M^{004}_{2,2} = -\frac{q}{16\,\pi^4\,m^2}\,\frac{3}{\nu_z^3}\,C_{004}; \qquad M^{012}_{2,2} \simeq \frac{q^2}{32\,\pi^6\,m^3}\,\frac{\eta_{\mathrm{m}}^2}{\nu_z^5}\,C_{012}^2. \tag{13}$$

$M^{012}_{2,2}$ is always positive, since it is proportional to the square of C_{012}, while $M^{004}_{2,2}$ can be positive or negative, depending on the sign of C_{004}. Hence, if an appropriate *optimal tuning ratio* can be found, such that the latter matrix element cancels the former, $T_{\mathrm{c}}^{\mathrm{opt}} \overset{?}{\longleftrightarrow} M^{012}_{2,2} + M^{004}_{2,2} = 0$, then the linear dependence of ν_z upon the axial energy can be eliminated.

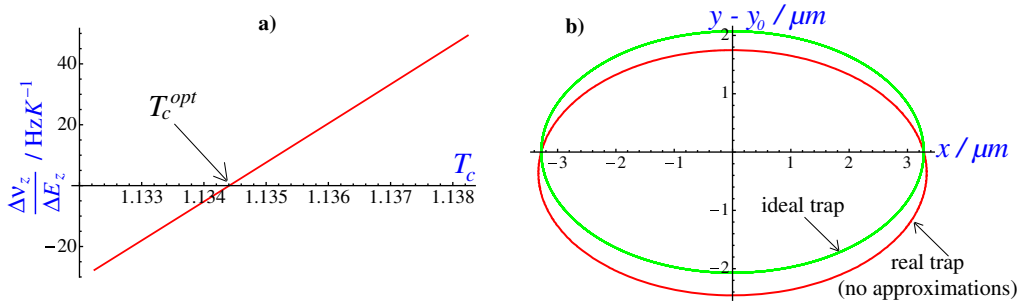

Figure 4. (a) Optimal tuning ratio, T_c^{opt} forcing $M_{2,2} = M_{2,2}^{004} + M_{2,2}^{012}$ to vanish. (b) Vertical shift of the magnetron ellipse with E_z due to C_{012}. For simplicity, the numerical computation of the real trap has been performed with $E_p \sim 0$.

The existence of T_c^{opt} cannot be universally guaranteed; however, it turns out that this is often the case. For the example trap, it can be seen in figure 4(a), where $\frac{\Delta\nu_z}{\Delta E_z}$ is plotted as a function of the applied T_c. One value, $T_c^{opt} = 1.134\,40$, eliminates $M_{2,2}$.

Since $\nu_z \propto C_{002}^{1/2}$, both frequency shifts in equation (13) equally scale with $V_r^{-1/2}$. The equation $M_{2,2}(T_c^{opt}) = 0$ is independent of the actual value of the ring potential and is solely defined by the voltage ratios T_c and T_e. A similar argument applies to the mass m and charge q. Thus, T_c^{opt} is a well-defined quantity, independent of V_r and of the trapped species. It does change with T_e, but this is simply equivalent to an inevitable dependence upon the trapping position y_0 (see section 3.4). The appearance of η_m in $M_{2,2}^{012}$ also implies that T_c^{opt} theoretically varies with the magnetic field; however, that dependence is negligible ($\sim -2 \times 10^{-6}\,T^{-1}$ for the example).

3.3. Physical origin of $M_{2,2}^{012}$

$M_{2,2}^{012}$ is due to the slight dependence of the trapping height on the axial energy, $y_0 = y_0(E_z)$. Indeed, for vanishing energy ($E_z = 0$) y_0 is the solution to the implicit equation $C_{010}(y_0) = 0$. For $E_z > 0$, that equation must be modified into $C_{010}(y_0') + \langle z^2\rangle \cdot C_{012}(y_0') = 0$. Here, $\langle z^2\rangle$ represents the time average of $A_z^2 \cos^2(\omega_z t)$. Thus, the real height, $y_0' = y_0 + \Delta y$, depends on the axial amplitude, and hence on E_z. Δy can be estimated as follows (we assume the approximation $C_{012}(y_0') \simeq C_{012}(y_0)$):

$$\left\{C_{010}(y_0') + \langle z^2\rangle\, C_{012}(y_0')\right\} - C_{010}(y_0) = 0 \rightarrow \underbrace{\frac{C_{010}(y_0+\Delta y) - C_{010}(y_0)}{\Delta y}}_{\simeq 2\,C_{020}} \Delta y + \langle z^2\rangle\, C_{012}(y_0) = 0$$

$$\Longrightarrow \quad \Delta y = -\frac{1}{2}\frac{C_{012}}{C_{020}}\langle z^2\rangle = \left(A_z^2\langle\cos^2(\omega_z t)\rangle = \frac{E_z}{m\,\omega_z^2}\right) = -\frac{1}{8\,\pi^2\,m\,\nu_z^2}\cdot\frac{C_{012}}{C_{020}}\,E_z. \tag{14}$$

At $y_0 + \Delta y$, the axial potential is modified with respect to y_0. In particular, the $E_z = 0$ axial curvature, $C_{002}(y_0)$, changes to $C_{002}'(y_0')$. This subsequently forces the variation of ω_z as a function of E_z:

$$\Delta\omega_z = \frac{\partial\omega_z}{\partial y}\cdot\Delta y = \frac{q}{m}\frac{1}{\sqrt{\frac{2\,q\,C_{002}}{m}}}\underbrace{\frac{\partial C_{002}}{\partial y}}_{C_{012}}\Delta y \quad\Longrightarrow\quad \frac{\Delta\nu_z}{\Delta E_z} = -\frac{q^2\,C_{012}^2}{32\,\pi^6\,m^3\,\nu_z^5}\left(\frac{C_{002}}{2\,C_{020}}\right). \tag{15}$$

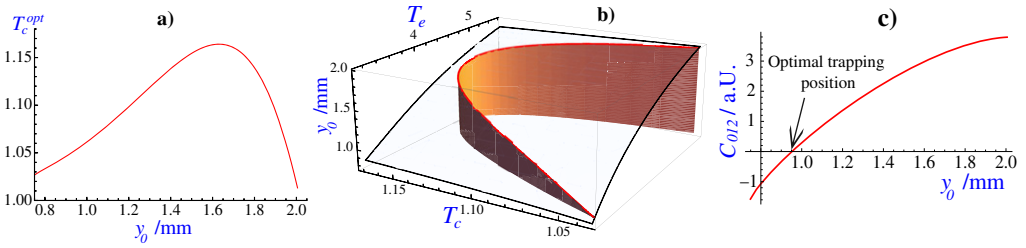

Figure 5. (a) Required optimal tuning ratio as a function of height y_0. (b) General variation of y_0 as a function of T_c, T_e. One particular path, $y_0 = y_0(T_e, T_c^{opt})$ (highlighted), corresponds to the compensated axial potential. (c) Plot of the vertical anharmonicity C_{012} along the compensated path.

The model described can be tested by computing numerically the radial motion of an electron in a real CPW-Penning trap, using $\phi(x, y, z)$ of equation (1) without approximations. The numerical calculation shows a vertical shift of the radial ellipse relative to the ideal one. An example, based upon the trap of section 2.1.1, is plotted in figure 4(b). This has been computed assuming $E_z = 4.2\,\mathrm{K}$, $E_m = -E_z(\nu_m/\nu_z)$ and $E_p \sim 0$. The shift predicted by equation (14) amounts to $\Delta y = -0.355\,\mu\mathrm{m}$ and is in good agreement with the numerical result of $\Delta y = -0.325\,\mu\mathrm{m}$. For low ellipticity, $\epsilon \to 0 \Rightarrow \eta_m^2 \to 1$ and $\frac{C_{002}}{2C_{020}} \to -1$ (see equation (4)). In this case, equations (15) and (13) (right) become identical. The former is actually accurate only for moderate values of ϵ, below ~ 0.5. Otherwise, it delivers shifts increasingly bigger than those predicted by the rigorous equation (13). In the limit $\epsilon \to +1 \Rightarrow \eta_m \to 0$ [24] and, as predicted by that equation, the effect of C_{012} upon ν_z is theoretically cancelled.

3.4. Compensation for different trapping heights

An optimal tuning ratio can be found within a continuous interval of trapping heights; however, it varies smoothly as a function of y_0. This is shown in figure 5(a), where the plot of T_c^{opt} versus y_0 is presented. A 'useful' interval exists ($0.8 \leqslant y_0 \leqslant 2\,\mathrm{mm}$ for the example), where $M_{2,2}$ can be eliminated. Beyond the upper or lower bounds of that interval, the optimal tuning ratio does not exist.

As shown in figure 5(b), T_c and T_e can be tuned independently and multiple combinations can be found to obtain one particular trapping position. However, the compensated interval is determined by a univocal relationship, $y_0 \Leftrightarrow (T_e, T_c^{opt})$, as featured in that graph. It must also be noted that T_e is the main parameter for changing y_0, while $1.2 \geqslant T_c \geqslant 1$, and the latter is basically used for compensation.

3.4.1. Optimal trapping position y_0^{012}. Figure 5(c) shows variation of C_{012} with the trapping position. At $y_0 \simeq 0.95\,\mathrm{mm}$, C_{012} vanishes. In this case, the compensation of $\frac{\Delta\nu_z}{\Delta E_z}$ also implies that C_{004} will disappear. Hence, within the compensated interval, an optimal trapping position can be found, y_0^{012}, for which $C_{012} = C_{004} = 0$.

3.5. Effect of ellipticity upon compensation

For a circular trap (such as the cylindrical or the Mainz/Harvard planar traps [9, 12]), the symmetry of x and y implies that $C_{202} = C_{022}$. Thus, if $C_{004} = 0$, the constraints of equation (5) force all other octupole terms, C_{202}, C_{022}, C_{400}, C_{040} and C_{220}, to vanish simultaneously. For

an elliptical trap, though, x and y are not indistinguishable: if $C_{004} = 0$, that only implies that $C_{202} = -C_{022}$, but in general they will not disappear. The same argument applies to the case $C_{012} = 0$ and the coefficients C_{210} and C_{030}. For these reasons, even when $C_{004} = C_{012} = 0$, the matrix M will always contain some elements different from 0. An ideal elliptical trap cannot be exactly approximated with a CPW-Penning trap. The non-vanishing elements are basically the shifts produced by E_p (first column of M) and those due to E_m (third column).

3.5.1. Shifts due to E_p. It can be shown that for all y_0 within the compensated interval, the frequency shifts produced by the cyclotron and magnetron energies are of the same order of magnitude as in the example of equation (12). Thus, if E_p is in the cryogenic domain ($E_\mathrm{p} \sim 4.2\,\mathrm{K}$), the corresponding deviations of ν_p and ν_m are in the range of a few μHz, and of a few mHz for ν_z. The resulting relative uncertainties in any of the frequencies are negligible. Increasing the magnetic field would make those shifts even smaller (see appendix B). Therefore, the first column in M can always be ignored.

3.5.2. Shifts due to E_m. The numbers in the third column of equation (12) are apparently more significant. However, applying sideband cooling [2, 28, 29], the magnetron energy takes the value $E_\mathrm{m} = -E_z(\nu_\mathrm{m}/\nu_z)$, which is in the range of a few mK (if $E_z \sim 4.2\,\mathrm{K}$). Since the magnetron energy does not fluctuate in time [2], the resulting frequency shifts represent mere offsets—which can be corrected for—without affecting the 'visibility' of the trapped particle (see section 3.8). In the example, the biggest relative offset would be $\sim 10^{-7}$ for ν_z, propagating to $\sim 10^{-12}$ in ν_c. Increasing the magnetic field, or the applied ring voltage, reduces further the third column of M (see appendix B).

3.6. First-order nonlinear anharmonicities

After eliminating the linear dependence of the axial frequency upon E_z, nonlinear shifts might still be important, especially when y_0 is small. The next most significant even anharmonicities, whose effect can be calculated by *first-order* perturbation theory, are C_{006} and C_{008}. These produce the following quadratic and cubic shifts, respectively:

$$\Delta\nu_z = \frac{15\,q}{128\,\pi^6\,m^3}\,\frac{C_{006}}{\nu_z^5}\cdot(\Delta E_z)^2; \qquad \Delta\nu_z = \frac{140\,q}{2048\,\pi^8\,m^4}\,\frac{C_{008}}{\nu_z^7}\cdot(\Delta E_z)^3. \tag{16}$$

For the example trap, these nonlinear shifts are shown in figure 6.

3.7. Second-order nonlinear anharmonicities

The next most significant odd anharmonicities, after those included in equation (3), are C_{014}, C_{212}, C_{032}, C_{410}, C_{230} and C_{050} ($\leftrightarrow i + j + k = 5$). The calculation of the corresponding frequency shifts, with rigorous *second-order* perturbation theory, would be extremely cumbersome. Instead, we employ the model presented in section 3.3. Following the derivation of equations (14)–(15), we obtain

$$\Delta\nu_z = -\frac{3\,q}{128\,\pi^6\,m^3\,\nu_z^5}\,\frac{C_{012}\cdot C_{014}}{C_{020}}\cdot(\Delta E_z)^2, \tag{17}$$

$$\Delta\nu_z = -\frac{q}{128\,\pi^6\,m^3\,\nu_z^3}\,\frac{C_{012}\cdot C_{212}}{C_{020}}\cdot\Delta E_z\left(\frac{\xi_\mathrm{p}^2}{\gamma_\mathrm{p}\,\nu_\mathrm{p}^2}\,\Delta E_\mathrm{p} + \frac{\xi_\mathrm{m}^2}{\nu_\mathrm{m}^2 - \nu_z^2/2}\,\Delta E_\mathrm{m}\right). \tag{18}$$

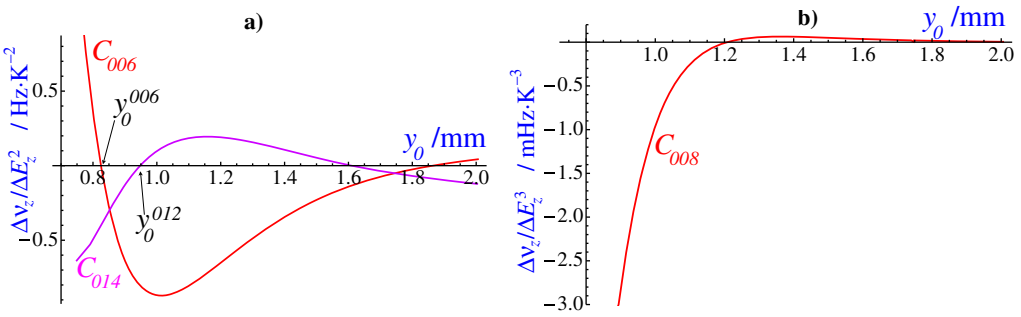

Figure 6. (a) Plot of the quadratic axial frequency shifts produced by C_{006} and C_{014} along $y_0 = y_0(T_e, T_c^{opt})$. Notice the positions y_0^{006} and y_0^{012}, where C_{006} and C_{012} respectively cancel. (b) Plot of the shift due to C_{008} along the compensated path.

The shift predicted by equation (17) has a similar magnitude to that produced by C_{006} (see figure 6 (a)). It must be taken into account when designing a CPW-trap. Note that equations (17) (and 18) vanish at y_0^{012}.

Equation (18) predicts a frequency shift scaling with the products $\Delta E_z \cdot \Delta E_p$ and $\Delta E_z \cdot \Delta E_m$. In the former case, the shift is proportional to $1/\nu_p^2$; hence, it is normally negligible. In the latter case, as already discussed, ΔE_m is very small and the corresponding value of $\Delta\nu_z$ is also inappreciable. Thus, C_{212} can be ignored. The same arguments apply to C_{032}, which produces a shift very similar to equation (18) ($\xi_{p,m}$ must be simply substituted by $\eta_{p,m}$). The remaining fifth-order coefficients, C_{410}, C_{230} and C_{050}, generate only deviations of ν_p and ν_m with products of ΔE_p and ΔE_m. Therefore, as explained in section 3.5.1 and 3.5.2, they can be ignored too. Finally, similar arguments apply to all sixth-order coefficients that have not been considered in section 3.6, namely C_{222}, C_{204}, C_{024}, C_{420}, C_{402}, C_{042}, C_{240}, C_{600} and C_{060}; they are all irrelevant.

3.7.1. Optimization of the compensation electrode. Figure 6(a) reveals the existence of one particular position, $y_0^{006} \simeq 0.83$ mm, at which $C_{006} = 0$. The question that arises is whether the trap can be designed to make y_0^{006} and y_0^{012} coincident. The answer is affirmative and is illustrated in figure 7. It shows the variation of y_0^{012} and y_0^{006} when changing the length of the compensation electrode, l_c, while keeping all other dimensions of the trap constant. For example, when $l_c \simeq 1.75$ mm $\Rightarrow y_0^{012} = y_0^{006} \simeq 0.82$ mm. For this optimized trap, $C_{004} = C_{012} = C_{006} = 0$, at y_0^{012}.

3.8. Observation of a single trapped electron

With the dependence $\nu_z = \nu_z(E_z, E_z^2, E_z^3)$ given in equations (13), (16) and (17), we are now in a position to perform a realistic simulation of the axial signal of a trapped electron. We assume the detection scheme employed in [30, 31], where the signal appears as a shortcut (= the axial dip) of the resonance resistance of a parallel LC-circuit. The goal is to compare the actual signal in the real trap to the ideal one, with the purpose of estimating the 'relative visibility' of the former. The technical details are therefore unimportant; however, they can be found in [32, 33]. The simulations are shown in figure 8. The curves are obtained by averaging the axial *dip* (with

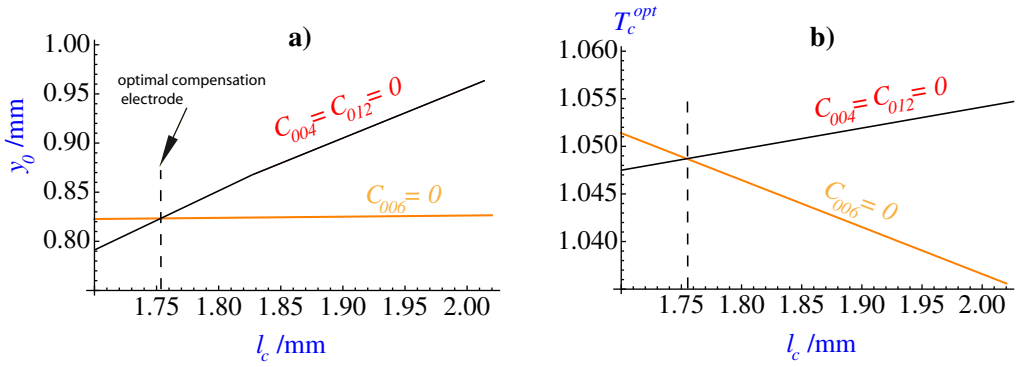

Figure 7. (a) Plot of y_0^{012} and y_0^{006} as a function of length of the compensation electrodes. Notice that y_0^{006} changes very slowly as a function of l_c. (b) Plot of the corresponding required optimal tuning ratio.

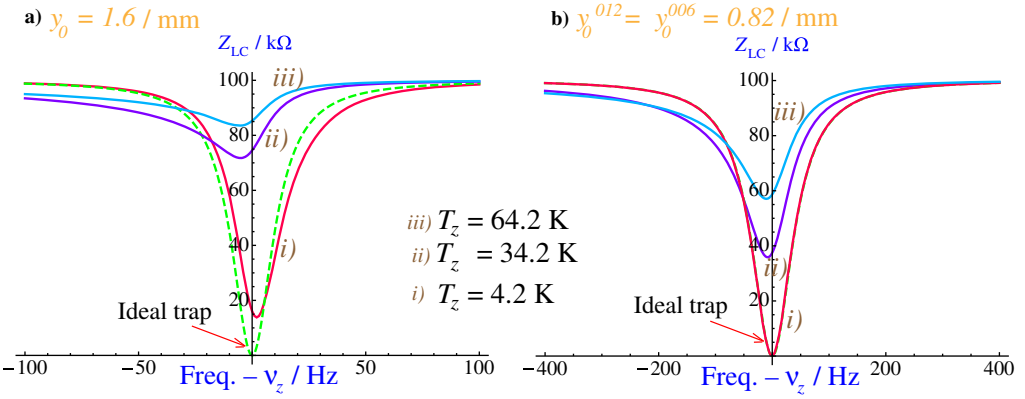

Figure 8. Axial *dip* of a single electron in the example trap with optimized l_c. The detection LC-circuit is assumed to be perfectly resonant with the electron's axial frequency and with a resonance resistance of $Z_{LC} = 100\,\mathrm{k\Omega}$. It is also assumed that the signal is picked up from one of the compensation electrodes. The difference in the widths of the ideal dips in panels (a) and (b) is caused by the variation of the induced signal with y_0. In panel (b) the ideal dip and the real one at 4.2 K are indistinguishable.

$\nu_z = \nu_z(E_z, E_z^2, E_z^3)$) over a Boltzmann distribution of the axial energy [27]. Three different values of the axial temperature T_z have been analysed.

Figure 8 shows the reduction of the 'visibility' of the dips with increasing axial temperature. A random position, $y_0 = 1.6\,\mathrm{mm}$ (but with optimized tuning ratio), has been chosen for plot (a). In this case, C_{006} and C_{014} produce the increasing deterioration of the dip, while C_{008} is negligible (see figure 6). In plot (b), $y_0 = y_0^{012} = y_0^{006} = 0.82\,\mathrm{mm}$ (see figure 7). Now, $C_{004} = C_{012} = C_{006} = 0$; however, C_{008} still diminishes the quality of the signal with T_z. It can be concluded that the detection of a single electron at 4.2 K (or lower) should always be possible within the compensated interval. However, for increasing temperatures the nonlinear anharmonicities make its observation significantly more difficult, even for relatively modest values of T_z. Besides fabrication and materials issues [12], those anharmonicities represent one of the main limits to the scalability of the CPW-Penning trap, since they inevitably increase for smaller y_0.

4. Summary and conclusions

For the sake of clarity, the discussion has been illustrated with the help of a concrete example. According to it, the main properties of the CPW-Penning trap can be summarized as follows.

- The existence of a trapping interval where the linear dependence of the axial frequency on the axial energy can be eliminated by appropriately tuning the voltage of the compensation electrodes.
- The existence of a particular position within the compensated interval, y_0^{012}, where the main anharmonicities, C_{012} and C_{004}, simultaneously vanish.
- The optimization of the compensation electrode, permitting the further elimination of C_{006} at the optimal trapping position.

Although these properties do not universally apply to all conceivable CPW-traps (in particular, the existence of y_0^{012} and/or y_0^{006}), they are indeed quite common: many examples can be presented—covering a very wide range of possible trap dimensions and aspect ratios—which do exhibit the characteristics listed. Thus, these might generally serve as a practical guidance in the process of designing a CPW-Penning trap for a particular application.

The potential integration of a geonium atom into future circuit-QED applications has been one of the main motivations for the development of the CPW-Penning trap. However, it offers many other interesting possibilities, such as the achievement of an *extremely elliptical* ($\epsilon \to +1$) 'quasi-2D' regime for electrons in free space, similar to that of high electron mobility transistors, graphene and other systems. These and other options will be discussed in detail in future papers.

Acknowledgments

The author acknowledges financial support from EPSRC, under grant no. EP/I012850/1, from the Marie Curie reintegration grant 'NGAMIT' and from SEPnet.

Appendix A. Calculation of electrostatic trapping potential

The Green's function for the Laplace equation with Dirichlet's boundary conditions in an infinite plane ($y = 0$) is [34] $G(\vec{r}\,|\,\vec{r}\,') = \frac{1}{\sqrt{(x-x')^2+(y-y')^2+(z-z')^2}} - \frac{1}{\sqrt{(x-x')^2+(y+y')^2+(z-z')^2}}$, and the potential is $\phi(x, y, z) = -\frac{1}{4\pi}\int_{-S_0/2}^{S_0/2} \mathrm{d}x' \int_{-L_0/2}^{L_0/2} \mathrm{d}z'\, V(x', 0, z') \cdot \frac{\partial\, G(\vec{r}\,|\,\vec{r}\,')}{\partial\, y'}|_{y'=0}$. For simplicity, we assume that the slit between the ground planes and the central strip is infinitely small. Thus, the boundary conditions are independent of $x' \to V(x', 0, z') = V(z')$. The integral along the electrodes delivers the following functions:

$$
\begin{aligned}
f_\mathrm{r}(x, y, z) &= f_0(x, y, z, l_\mathrm{r}/2) - f_0(x, y, z, -l_\mathrm{r}/2),\\
f_\mathrm{c}(x, y, z) &= f_0(x, y, z, z_\mathrm{up}^\mathrm{c}) - f_0(x, y, z, z_\mathrm{low}^\mathrm{c}) + f_0(x, y, z, -z_\mathrm{low}^\mathrm{c}) - f_0(x, y, z, -z_\mathrm{up}^\mathrm{c}),\\
f_\mathrm{e}(x, y, z) &= f_0(x, y, z, z_\mathrm{up}^\mathrm{e}) - f_0(x, y, z, z_\mathrm{low}^\mathrm{e}) + f_0(x, y, z, -z_\mathrm{low}^\mathrm{e}) - f_0(x, y, z, -z_\mathrm{up}^\mathrm{e}),\\
f_0(x, y, z, z') &= \frac{1}{2\pi}\left\{\arctan\left(\frac{\left(x-\frac{S_0}{2}\right)(z-z')}{y\sqrt{\left(x-\frac{S_0}{2}\right)^2+y^2+(z-z')^2}}\right) - \arctan\left(\frac{\left(x+\frac{S_0}{2}\right)(z-z')}{y\sqrt{\left(x+\frac{S_0}{2}\right)^2+y^2+(z-z')^2}}\right)\right\}.
\end{aligned}
\tag{A.1}
$$

In equation (A.2), the upper limit of the compensation electrode is $z^{\mathrm{c}}_{\mathrm{up}} = l_{\mathrm{c}} + \eta + l_{\mathrm{r}}/2$ and the lower one is $z^{\mathrm{c}}_{\mathrm{low}} = \eta + l_{\mathrm{r}}/2$. For the end-cap, the upper limit is $z^{\mathrm{e}}_{\mathrm{up}} = l_{\mathrm{e}} + l_{\mathrm{c}} + 2\eta + l_{\mathrm{r}}/2$ and the lower one is $z^{\mathrm{e}}_{\mathrm{low}} = l_{\mathrm{c}} + 2\eta + l_{\mathrm{r}}/2$.

The gaps between electrodes modify the pure Dirichlet's problem into a much more complex one, involving also Neumann boundary conditions. A rigorous analytic solution (if possible) would demand the use of highly sophisticated mathematical techniques [34]. In order to avoid this mathematical complexity, we approximate the boundary conditions across any of the insulating gaps (which are *a priori* unknown) by a linear interpolation between the two dc-voltages applied to the corresponding electrodes: $V(z') = m\,z' + n$. Here m, n depend on the particular gap. The linear interpolation approximation is acceptable as long as the width of the gaps, η, is small compared to the dimensions of the electrodes (see [22] and references therein). The result is

$$
\begin{aligned}
f_{\mathrm{gaps}}(\vec{r} \mid V_{\mathrm{r}}, V_{\mathrm{c}}, V_{\mathrm{e}}) = {} & f_1\left(\vec{r}, z^{\mathrm{c}}_{\mathrm{low}}, \frac{V_{\mathrm{c}} - V_{\mathrm{r}}}{\eta}, V_{\mathrm{r}} - \frac{l_{\mathrm{r}}(V_{\mathrm{r}} - V_{\mathrm{c}})}{2\eta}\right) - f_1\left(\vec{r}, l_{\mathrm{r}}/2, \frac{V_{\mathrm{c}} - V_{\mathrm{r}}}{\eta}, V_{\mathrm{r}}\right. \\
& \left. - \frac{l_{\mathrm{r}}(V_{\mathrm{r}} - V_{\mathrm{c}})}{2\eta}\right) + f_1\left(\vec{r}, -l_{\mathrm{r}}/2, -\frac{V_{\mathrm{c}} - V_{\mathrm{r}}}{\eta}, V_{\mathrm{r}} - \frac{l_{\mathrm{r}}(V_{\mathrm{r}} - V_{\mathrm{c}})}{2\eta}\right) \\
& - f_1\left(\vec{r}, -z^{\mathrm{c}}_{\mathrm{low}}, -\frac{V_{\mathrm{c}} - V_{\mathrm{r}}}{\eta}, V_{\mathrm{r}} - \frac{l_{\mathrm{r}}(V_{\mathrm{r}} - V_{\mathrm{c}})}{2\eta}\right) + f_1\left(\vec{r}, z^{\mathrm{e}}_{\mathrm{low}}, \frac{V_{\mathrm{e}} - V_{\mathrm{c}}}{\eta}, V_{\mathrm{c}}\right. \\
& \left. - \frac{(V_{\mathrm{e}} - V_{\mathrm{c}})\, z^{\mathrm{c}}_{\mathrm{low}}}{\eta}\right) - f_1\left(\vec{r}, z^{\mathrm{c}}_{\mathrm{up}}, \frac{V_{\mathrm{e}} - V_{\mathrm{c}}}{\eta}, V_{\mathrm{c}} - \frac{(V_{\mathrm{e}} - V_{\mathrm{c}})\, z^{\mathrm{c}}_{\mathrm{low}}}{\eta}\right) \\
& + f_1\left(\vec{r}, -z^{\mathrm{c}}_{\mathrm{up}}, -\frac{V_{\mathrm{e}} - V_{\mathrm{c}}}{\eta}, V_{\mathrm{c}} - \frac{(V_{\mathrm{e}} - V_{\mathrm{c}})\, z^{\mathrm{c}}_{\mathrm{low}}}{\eta}\right) \\
& - f_1\left(\vec{r}, -z^{\mathrm{e}}_{\mathrm{low}}, -\frac{V_{\mathrm{e}} - V_{\mathrm{c}}}{\eta}, V_{\mathrm{c}} - \frac{(V_{\mathrm{e}} - V_{\mathrm{c}})\, z^{\mathrm{c}}_{\mathrm{low}}}{\eta}\right) \\
& + f_1\left(\vec{r}, z^{\mathrm{e}}_{\mathrm{up}} + \eta, \frac{-V_{\mathrm{e}}}{\eta}, \frac{V_{\mathrm{e}}(z^{\mathrm{e}}_{\mathrm{up}} + \eta)}{\eta}\right) - f_1\left(\vec{r}, z^{\mathrm{e}}_{\mathrm{up}}, \frac{-V_{\mathrm{e}}}{\eta}, \frac{V_{\mathrm{e}}(z^{\mathrm{e}}_{\mathrm{up}} + \eta)}{\eta}\right) \\
& + f_1\left(\vec{r}, -z^{\mathrm{e}}_{\mathrm{up}}, \frac{V_{\mathrm{e}}}{\eta}, \frac{V_{\mathrm{e}}(z^{\mathrm{e}}_{\mathrm{up}} + \eta)}{\eta}\right) - f_1\left(\vec{r}, -z^{\mathrm{e}}_{\mathrm{up}} - \eta, \frac{V_{\mathrm{e}}}{\eta}, \frac{V_{\mathrm{e}}(z^{\mathrm{e}}_{\mathrm{up}} + \eta)}{\eta}\right). \qquad \text{(A.2)}
\end{aligned}
$$

The auxiliary function $f_1(\vec{r}, z', m, n)$ has the following form:

$$
\begin{aligned}
f_1(x, y, z, z', m, n) = {} & \frac{\mathrm{i}(m(z + \mathrm{i}y) + n)}{4\pi} \\
& \times \log\left(\frac{y\left(\mathrm{i}(S_0 - 2x)\left(S_0 - 2x + \sqrt{(S_0 - 2x)^2 + 4\left(y^2 + (z - z')^2\right)}\right) + 4y(z + \mathrm{i}y - z')\right)}{(S_0 - 2x)(-\mathrm{i}y - z + z')(m(z + \mathrm{i}y) + n)}\right) \\
& + \frac{\mathrm{i}(m(z + \mathrm{i}y) + n)}{4\pi} \\
& \times \log\left(\frac{y\left(\mathrm{i}(S_0 + 2x)\left(S_0 + 2x + \sqrt{(S_0 + 2x)^2 + 4\left(y^2 + (z - z')^2\right)}\right) + 4y(z + \mathrm{i}y - z')\right)}{(S_0 + 2x)(-\mathrm{i}y - z + z')(m(z + \mathrm{i}y) + n)}\right)
\end{aligned}
$$

$$
-\frac{\mathrm{i}(m(z-\mathrm{i}y)+n)}{4\pi}
\times\log\left(\frac{y\left(-\mathrm{i}(S_0-2x)\left(S_0-2x+\sqrt{(S_0-2x)^2+4\left(y^2+(z-z')^2\right)}\right)+4y(z-\mathrm{i}y-z')\right)}{(S_0-2x)(\mathrm{i}y-z+z')(m(z-\mathrm{i}y)+n)}\right)
$$

$$
-\frac{\mathrm{i}(m(z-\mathrm{i}y)+n)}{4\pi}
\times\log\left(\frac{y\left(-\mathrm{i}(S_0+2x)\left(S_0+2x+\sqrt{(S_0+2x)^2+4\left(y^2+(z-z')^2\right)}\right)+4y(z-\mathrm{i}y-z')\right)}{(S_0+2x)(\mathrm{i}y-z+z')(m(z-\mathrm{i}y)+n)}\right). \tag{A.3}
$$

Appendix B. Frequency-shifts matrices

The frequency-shifts matrices are calculated following [35]. Even anharmonicities (C_{ijk} with j even and $i+j+k>2$) are treated with *first-order canonical perturbation theory*. This simply requires averaging the perturbation Hamiltonian over an oscillation period of the trapped particle [24, 35]. On the other hand, the perturbation Hamiltonian of any odd C_{ijk} (j is odd) averages to zero. Thus, those anharmonicities must be treated with *second-order perturbation theory* methods. The latter require the solution of the Hamilton–Jacobi equation for the perturbative Hamiltonian. The frequency shifts are derived from that solution [35].

$$
M^{004}=\frac{q\,C_{004}}{16\,\pi^4\,m^2\,\nu_z^3}\cdot\begin{pmatrix}0&0&0\\0&3&0\\0&0&0\end{pmatrix}. \tag{B.1}
$$

$$
M^{220}=\frac{q\,C_{220}}{16\,\pi^4\,m^2\,\nu_\mathrm{p}}\cdot\begin{pmatrix}\frac{\eta_\mathrm{p}^2\,\xi_\mathrm{p}^2}{\gamma_\mathrm{p}^2\,\nu_\mathrm{p}^2}&0&\frac{\left(\xi_\mathrm{m}^2\eta_\mathrm{p}^2+\eta_\mathrm{m}^2\xi_\mathrm{p}^2\right)}{\gamma_\mathrm{p}\left(\nu_\mathrm{m}^2-\nu_z^2/2\right)}\\0&0&0\\\frac{\nu_\mathrm{m}\left(\xi_\mathrm{m}^2\eta_\mathrm{p}^2+\eta_\mathrm{m}^2\xi_\mathrm{p}^2\right)}{\gamma_\mathrm{p}\,\nu_\mathrm{p}\left(\nu_\mathrm{m}^2-\nu_z^2/2\right)}&0&\frac{\nu_\mathrm{m}\,\nu_\mathrm{p}\,\eta_\mathrm{m}^2\,\xi_\mathrm{m}^2}{\left(\nu_\mathrm{m}^2-\nu_z^2/2\right)^2}\end{pmatrix}. \tag{B.2}
$$

$$
M^{202}=\frac{q\,C_{202}}{16\,\pi^4\,m^2\,\nu_z}\cdot\begin{pmatrix}0&\frac{\xi_\mathrm{p}^2}{\gamma_\mathrm{p}\,\nu_\mathrm{p}\,\nu_z}&0\\\frac{\xi_\mathrm{p}^2}{\gamma_\mathrm{p}\,\nu_\mathrm{p}^2}&0&\frac{\xi_\mathrm{m}^2}{\left(\nu_\mathrm{m}^2-\nu_z^2/2\right)}\\0&\frac{\nu_\mathrm{m}\,\xi_\mathrm{m}^2}{\nu_z\left(\nu_\mathrm{m}^2-\nu_z^2/2\right)}&0\end{pmatrix}. \tag{B.3}
$$

$$
M^{022}=\frac{q\,C_{022}}{16\,\pi^4\,m^2\,\nu_z}\cdot\begin{pmatrix}0&\frac{\eta_\mathrm{p}^2}{\gamma_\mathrm{p}\,\nu_\mathrm{p}\,\nu_z}&0\\\frac{\eta_\mathrm{p}^2}{\gamma_\mathrm{p}\,\nu_\mathrm{p}^2}&0&\frac{\eta_\mathrm{m}^2}{\left(\nu_\mathrm{m}^2-\nu_z^2/2\right)}\\0&\frac{\nu_\mathrm{m}\,\eta_\mathrm{m}^2}{\nu_z\left(\nu_\mathrm{m}^2-\nu_z^2/2\right)}&0\end{pmatrix}. \tag{B.4}
$$

$$M^{400} = \frac{q\,C_{400}}{16\,\pi^4\,m^2\,\nu_\mathrm{p}} \cdot \begin{pmatrix} \frac{3\,\xi_\mathrm{p}^4}{\gamma_\mathrm{p}^2\,\nu_\mathrm{p}^2} & 0 & \frac{6\,\xi_\mathrm{m}^2\,\xi_\mathrm{p}^2}{\gamma_\mathrm{p}\left(\nu_\mathrm{m}^2-\nu_z^2/2\right)} \\ 0 & 0 & 0 \\ \frac{6\,\xi_\mathrm{m}^2\,\xi_\mathrm{p}^2\,\nu_\mathrm{m}}{\gamma_\mathrm{p}\,\nu_\mathrm{p}\left(\nu_\mathrm{m}^2-\nu_z^2/2\right)} & 0 & \frac{3\,\xi_\mathrm{m}^4\,\nu_\mathrm{m}\,\nu_\mathrm{p}}{\left(\nu_\mathrm{m}^2-\nu_z^2/2\right)^2} \end{pmatrix}. \tag{B.5}$$

$$M^{040} = \frac{q\,C_{040}}{16\,\pi^4\,m^2\,\nu_\mathrm{p}} \cdot \begin{pmatrix} \frac{3\,\eta_\mathrm{p}^4}{\gamma_\mathrm{p}^2\,\nu_\mathrm{p}^2} & 0 & \frac{6\,\eta_\mathrm{m}^2\eta_\mathrm{p}^2}{\gamma_\mathrm{p}\left(\nu_\mathrm{m}^2-\nu_z^2/2\right)} \\ 0 & 0 & 0 \\ \frac{6\,\eta_\mathrm{m}^2\,\eta_\mathrm{p}^2\,\nu_\mathrm{m}}{\gamma_\mathrm{p}\,\nu_\mathrm{p}\left(\nu_\mathrm{m}^2-\nu_z^2/2\right)} & 0 & \frac{3\,\eta_\mathrm{m}^4\,\nu_\mathrm{m}\,\nu_\mathrm{p}}{\left(\nu_\mathrm{m}^2-\nu_z^2/2\right)^2} \end{pmatrix}. \tag{B.6}$$

$$M^{012} = \frac{q^2\,C_{012}^2}{32\,\pi^6\,m^3\,\nu_z^2} \cdot \begin{pmatrix} 0 & \frac{\eta_\mathrm{p}^2}{\gamma_\mathrm{p}\,\nu_\mathrm{p}\left(\nu_\mathrm{p}^2-4\,\nu_z^2\right)} & 0 \\ \frac{\eta_\mathrm{p}^2\,\nu_z}{\gamma_\mathrm{p}\,\nu_\mathrm{p}^2\left(\nu_\mathrm{p}^2-4\,\nu_z^2\right)} & -\frac{\eta_\mathrm{m}^2\left(3\,\nu_\mathrm{m}^2-8\,\nu_z^2\right)}{4\,\nu_z\left(\nu_\mathrm{m}^2-4\,\nu_z^2\right)\left(\nu_\mathrm{m}^2-\nu_z^2/2\right)} - \frac{\eta_\mathrm{p}^2\left(3\,\nu_\mathrm{p}^2-8\,\nu_z^2\right)}{4\,\gamma_\mathrm{p}\,\nu_\mathrm{p}^2\,\nu_z\left(\nu_\mathrm{p}^2-4\,\nu_z^2\right)} & \frac{\eta_\mathrm{m}^2\,\nu_z}{\left(\nu_\mathrm{m}^2-4\,\nu_z^2\right)\left(\nu_\mathrm{m}^2-\nu_z^2/2\right)} \\ 0 & \frac{\eta_\mathrm{m}^2\,\nu_\mathrm{m}}{\left(\nu_\mathrm{m}^2-4\,\nu_z^2\right)\left(\nu_\mathrm{m}^2-\nu_z^2/2\right)} & 0 \end{pmatrix}. \tag{B.7}$$

$$M^{210} = \frac{q^2\,C_{210}^2}{32\,\pi^6\,m^3\,\gamma_\mathrm{p}^2\,\nu_\mathrm{p}^3} \cdot \begin{pmatrix} a_{1,1} & 0 & a_{1,3} \\ 0 & 0 & 0 \\ a_{3,1} & 0 & a_{3,3} \end{pmatrix} \tag{B.8}$$

$$a_{1,1} = -\frac{\xi_\mathrm{p}^2 \begin{pmatrix} 3\,\eta_\mathrm{p}^2\,\xi_\mathrm{p}^2\left(\nu_\mathrm{m}^2-4\nu_\mathrm{p}^2\right)\left(2\,\nu_\mathrm{m}^2-\nu_z^2\right)+2\,\gamma_\mathrm{p}\,\nu_\mathrm{p}^2(4\,\nu_\mathrm{m}^2\,\xi_\mathrm{m}^2\,\eta_\mathrm{p}^2 \\ -8\,\eta_\mathrm{m}\,\nu_\mathrm{m}\,\xi_\mathrm{m}\,\eta_\mathrm{p}\,\nu_\mathrm{p}\,\xi_\mathrm{p}+\eta_\mathrm{m}^2\,\xi_\mathrm{p}^2(3\nu_\mathrm{m}^2-8\nu_\mathrm{p}^2)) \end{pmatrix}}{4\,\gamma_\mathrm{p}\,\nu_\mathrm{p}^2\left(\nu_\mathrm{m}^2-4\nu_\mathrm{p}^2\right)\left(2\nu_\mathrm{m}^2-\nu_z^2\right)} \tag{B.9}$$

$$a_{3,1} = \frac{\nu_\mathrm{m}}{2(\nu_\mathrm{m}^2-\nu_z^2/2)} \left(\frac{\xi_\mathrm{p}^2\left(-\xi_\mathrm{m}^2\eta_\mathrm{p}^2\left(\nu_\mathrm{m}^2-12\nu_\mathrm{p}^2\right)-4\eta_\mathrm{m}\,\eta_\mathrm{p}\,\xi_\mathrm{m}\,\xi_\mathrm{p}\,\nu_\mathrm{m}\,\nu_\mathrm{p}+2\,\eta_\mathrm{m}^2\,\xi_\mathrm{p}^2\,\nu_\mathrm{p}^2\right)}{\nu_\mathrm{p}\left(\nu_\mathrm{m}^2-4\nu_\mathrm{p}^2\right)} \right.$$
$$\left. + \frac{\xi_\mathrm{m}^2\gamma_\mathrm{p}\,\nu_\mathrm{p}\left(4\,\eta_\mathrm{m}\,\xi_\mathrm{m}\eta_\mathrm{p}\,\xi_\mathrm{p}\,\nu_\mathrm{m}\,\nu_\mathrm{p}+\eta_\mathrm{m}^2\,\xi_\mathrm{p}^2\left(\nu_\mathrm{p}^2-12\nu_\mathrm{m}^2\right)-2\,\nu_\mathrm{m}^2\,\xi_\mathrm{m}^2\,\eta_\mathrm{p}^2\right)}{\left(4\nu_\mathrm{m}^2-\nu_\mathrm{p}^2\right)\left(\nu_\mathrm{m}^2-\frac{\nu_z^2}{2}\right)} \right) \tag{B.10}$$

$$a_{1,3} = \frac{1}{2(\nu_\mathrm{m}^2-\nu_z^2/2)} \left(\frac{\xi_\mathrm{p}^2\left(\xi_\mathrm{m}^2\left(-\eta_\mathrm{p}^2\right)\left(\nu_\mathrm{m}^2-12\nu_\mathrm{p}^2\right)-4\,\eta_\mathrm{m}\,\xi_\mathrm{m}\,\eta_\mathrm{p}\,\xi_\mathrm{p}\,\nu_\mathrm{m}\,\nu_\mathrm{p}+2\eta_\mathrm{m}^2\,\nu_\mathrm{p}^2\,\xi_\mathrm{p}^2\right)}{\nu_\mathrm{p}\left(\nu_\mathrm{m}^2-4\nu_\mathrm{p}^2\right)} \right.$$
$$\left. + \frac{2\,\xi_\mathrm{m}^2\,\gamma_\mathrm{p}\,\nu_\mathrm{p}\left(4\,\eta_\mathrm{m}\,\xi_\mathrm{m}\,\eta_\mathrm{p}\,\xi_\mathrm{p}\,\nu_\mathrm{m}\nu_\mathrm{p}+\eta_\mathrm{m}^2\,\xi_\mathrm{p}^2\left(\nu_\mathrm{p}^2-12\nu_\mathrm{m}^2\right)-2\,\nu_\mathrm{m}^2\,\xi_\mathrm{m}^2\,\eta_\mathrm{p}^2\right)}{\left(4\nu_\mathrm{m}^2-\nu_\mathrm{p}^2\right)\left(2\nu_\mathrm{m}^2-\nu_z^2\right)} \right) \tag{B.11}$$

$$a_{3,3} = \frac{\begin{pmatrix} \nu_\mathrm{m}\xi_\mathrm{m}^2\gamma_\mathrm{p}\nu_\mathrm{p}(2\nu_\mathrm{m}^2-\nu_z^2)^3(2\eta_\mathrm{m}^2\nu_\mathrm{p}^2(2\xi_\mathrm{p}^2(\nu_z^2-2\nu_\mathrm{m}^2)+3\xi_\mathrm{m}^2\gamma_\mathrm{p}(4\nu_\mathrm{m}^2-\nu_\mathrm{p}^2)) \\ +8\eta_\mathrm{m}\nu_\mathrm{m}\xi_\mathrm{m}\eta_\mathrm{p}\nu_\mathrm{p}\xi_\mathrm{p}(2\nu_\mathrm{m}^2-\nu_z^2)+\xi_\mathrm{m}^2\eta_\mathrm{p}^2(8\nu_\mathrm{m}^2-3\nu_\mathrm{p}^2)(2\nu_\mathrm{m}^2-\nu_z^2)) \end{pmatrix}}{\nu_\mathrm{p}^2-4\nu_\mathrm{m}^2} \tag{B.12}$$

$$M^{030} = \frac{q^2\, C_{030}^2}{32\,\pi^6\, m^3\, \nu_{\mathrm{p}}^3} \cdot \begin{pmatrix} b_{1,1} & 0 & b_{1,3} \\ 0 & 0 & 0 \\ b_{3,1} & 0 & b_{3,3} \end{pmatrix}, \tag{B.13}$$

$$b_{1,1} = -\frac{3\,\eta_{\mathrm{p}}^4}{4\,\gamma_{\mathrm{p}}^3\,\nu_{\mathrm{p}}^2}\left(\frac{6\,\eta_{\mathrm{m}}^2\,\gamma_{\mathrm{p}}\,\nu_{\mathrm{p}}^2\,\left(3\,\nu_{\mathrm{m}}^2 - 8\,\nu_{\mathrm{p}}^2\right)}{\left(\nu_{\mathrm{m}}^2 - 4\,\nu_{\mathrm{p}}^2\right)\left(2\,\nu_{\mathrm{m}}^2 - \nu_z^2\right)} + 5\,\eta_{\mathrm{p}}^2\right);$$

$$b_{1,3} = -\frac{9\eta_{\mathrm{m}}^2\,\eta_{\mathrm{p}}^2(\eta_{\mathrm{p}}^2(-25\,\nu_{\mathrm{m}}^2\,\nu_{\mathrm{p}}^2 + 4\,\nu_{\mathrm{m}}^4 + 6\,\nu_{\mathrm{p}}^4)(2\,\nu_{\mathrm{m}}^2 - \nu_z^2) + 2\,\eta_{\mathrm{m}}^2\,\gamma_{\mathrm{p}}\,\nu_{\mathrm{p}}^2\,(-25\,\nu_{\mathrm{m}}^2\,\nu_{\mathrm{p}}^2 + 6\,\nu_{\mathrm{m}}^4 + 4\,\nu_{\mathrm{p}}^4))}{\gamma_{\mathrm{p}}^2(-17\,\nu_{\mathrm{m}}^2\,\nu_{\mathrm{p}}^2 + 4\,\nu_{\mathrm{m}}^4 + 4\,\nu_{\mathrm{p}}^4)(\nu_z^2 - 2\,\nu_{\mathrm{m}}^2)^2}, \tag{B.14}$$

$$b_{3,1} = -\frac{9\eta_{\mathrm{m}}^2\,\nu_{\mathrm{m}}\eta_{\mathrm{p}}^2(\eta_{\mathrm{p}}^2(-25\nu_{\mathrm{m}}^2\nu_{\mathrm{p}}^2 + 4\nu_{\mathrm{m}}^4 + 6\nu_{\mathrm{p}}^4)(2\nu_{\mathrm{m}}^2 - \nu_z^2) + 2\eta_{\mathrm{m}}^2\gamma_{\mathrm{p}}\nu_{\mathrm{p}}^2(-25\nu_{\mathrm{m}}^2\nu_{\mathrm{p}}^2 + 6\nu_{\mathrm{m}}^4 + 4\nu_{\mathrm{p}}^4))}{\gamma_{\mathrm{p}}^2\nu_{\mathrm{p}}(-17\nu_{\mathrm{m}}^2\nu_{\mathrm{p}}^2 + 4\nu_{\mathrm{m}}^4 + 4\nu_{\mathrm{p}}^4)(\nu_z^2 - 2\nu_{\mathrm{m}}^2)^2};$$

$$b_{3,3} = \frac{3\,\eta_{\mathrm{m}}^4\,\nu_{\mathrm{m}}\,\nu_{\mathrm{p}}^3}{\left(\nu_z^2 - 2\,\nu_{\mathrm{m}}^2\right)^3}\left(\frac{3\,\eta_{\mathrm{p}}^2\,\left(3\,\nu_{\mathrm{p}}^2 - 8\,\nu_{\mathrm{m}}^2\right)\left(2\,\nu_{\mathrm{m}}^2 - \nu_z^2\right)}{\gamma_{\mathrm{p}}\,\nu_{\mathrm{p}}^2\,\left(\nu_{\mathrm{p}}^2 - 4\,\nu_{\mathrm{m}}^2\right)} + 10\,\eta_{\mathrm{m}}^2\right). \tag{B.15}$$

References

[1] Van Dyck R S, Schwinberg P B and Dehmelt H G 1977 Precise measurements of axial, magnetron, cyclotron and spin-cyclotron-beat frequencies on an isolated 1-mev electron *Phys. Rev. Lett.* **38** 310

[2] Brown L S and Gabrielse G 1986 Geonium theory: physics of a single electron or ion in a Penning trap *Rev. Mod. Phys.* **58** 233–11

[3] Hanneke D, Fogwell S and Gabrielse G 2008 New measurement of the electron magnetic moment and the fine structure constant *Phys. Rev. Lett.* **100** 120801

[4] Beier T, Häffner H, Hermanspahn N, Karshenboim S G, Kluge H-J, Quint W, Stahl S, Verdú J and Werth G 2001 New determination of the electron's mass *Phys. Rev. Lett.* **88** 011603

[5] Ciaramicoli G, Marzoli I and Tombesi P 2001 Realization of a quantum algorithm using a trapped electron *Phys. Rev.* A **63** 052307

[6] Ciaramicoli G, Marzoli I and Tombesi P 2003 Scalable quantum processor with trapped electrons *Phys. Rev. Lett.* **91** 017901

[7] Ciaramicoli G, Marzoli I and Tombesi P 2004 Trapped electrons in vacuum for a scalable quantum processor *Phys. Rev.* A **70** 032301

[8] DiVincenzo D P 2000 The physical implementation of quantum computation *Fortschr. Phys.* **48** 771–83

[9] Stahl S, Galve F, Alonso J, Djekić S, Quint W, Valenzuela T, Verdú J, Vogel M and Werth G 2005 A planar Penning trap *Eur. Phys. J.* D **32** 139–46

[10] Galve F, Fernández P and Werth G 2006 Operation of a planar Penning trap *Eur. Phys. J.* D **40** 201–4

[11] Bushev P, Stahl S, Natali R, Marx G, Stachowska E, Werth G, Hellwig M and Schmidt-Kaler F 2008 Electrons in a cryogenic planar Penning trap and experimental challenges for quantum processing *Eur. Phys. J.* D **50** 97–102

[12] Goldman J and Gabrielse G 2010 Optimized planar Penning traps for quantum-information studies *Phys. Rev.* A **81** 052335

[13] Day P K, LeDuc H G, Mazin B A, Vayonakis A and Zmuidzinas J 2003 A broadband superconducting detector suitable for use in large arrays *Nature* **425** 817–21

[14] Wen C P 1969 Coplanar waveguide: a surface strip transmission line suitable for nonreciprocal gyromagnetic device applications *IEEE Trans. Microw. Theory Tech.* **MTT-17** 1087
[15] Blais A, Huang R-S, Wallraff A, Girvin S M and Schoelkopf R J 2004 Cavity quantum electrodynamics for superconducting electrical circuits: an architecture for quantum computation *Phys. Rev.* A **69** 062320
[16] Wallraff A, Schuster D I, Blais A, Frunzio L, Huang R-S, Majer J, Kumar S, Girvin S M and Schoelkopf R J 2004 Strong coupling of a single photon to a superconducting qubit using circuit quantum electrodynamics *Nature* **431** 162
[17] Gabrielse G and MacKintosh F C 1984 Cylindrical Penning traps with orthogonalized anharmonicity compensation *Int. J. Mass Spectrom. Ion Process.* **57** 1
[18] Schuster D I *et al* 2010 High-cooperativity coupling of electron-spin ensembles to superconducting cavities *Phys. Rev. Lett.* **105** 140501
[19] Verdú J, Zoubi H, Koller Ch, Majer J, Ritsch H and Schmiedmayer J 2009 Strong magnetic coupling of an ultracold gas to a superconducting waveguide cavity *Phys. Rev. Lett.* **103** 043603
[20] André A, DeMille D, Doyle J M, Lukin M D, Rabl P, Schoelkopf R J and Zoller P 2006 A coherent all-electrical interface between polar molecules and mesoscopic superconducting resonators *Nat. Phys.* **2** 636
[21] Gabrielse G 1983 Relaxation calculation of the electrostatic properties of compensated Penning traps with hyperbolic electrodes *Phys. Rev.* A **27** 2277–90
[22] Verdú J L, Kreim S, Blaum K, Kracke H, Quint W, Ulmer S and Walz J 2008 Calculation of electrostatic fields using quasi-Green's functions: application to the hybrid Penning trap *New J. Phys.* **10** 23
[23] Breitenfeldt M, Baruah S, Blaum K, Herlert A, Kretzschmar M, Martinez F, Marx G, Schweikhard L and Walsh N 2008 The elliptical Penning trap: experimental investigations and simulations *Int. J. Mass Spectrom.* **275** 34–44
[24] Kretzschmar M 2008 Theory of the elliptical Penning trap *Int. J. Mass Spectrom.* **275** 21–33
[25] Blaum K 2006 High-accuracy mass spectrometry with stored ions *Phys. Rep.* **425** 1–78
[26] Hermanspahn N, Häffner H, Kluge H-J, Quint W, Stahl S, Verdú J and Werth G 2000 Observation of the continuous Stern-Gerlach effect on an electron bound in an atomic ion *Phys. Rev. Lett.* **84** 427–30
[27] Djekic S, Alonso J, Kluge H-J, Quint W, Stahl S, Valenzuela T, Verdú J, Vogel M and Werth G 2004 Temperature measurement of a single ion in a Penning trap *Eur. Phys. J.* D **31** 451–7
[28] Itano W M, Bergquist J C, Bollinger J J and Wineland D J 1995 Cooling methods in ion traps *Phys. Scr.* **T59** 106–20
[29] Cornell E A, Weisskoff R M, Boyce K R and Pritchard D E 1990 Mode coupling in a Penning trap: π pulses and a classical avoided crossing *Phys. Rev.* A **41** 312–5
[30] Häffner H, Beier T, Hermanspahn N, Kluge H-J, Quint W, Stahl S, Verdú J and Werth G 2000 High-accuracy measurement of the magnetic moment anomaly of the electron bound in hydrogenlike carbon *Phys. Rev. Lett.* **85** 5308–11
[31] Verdú J, Djekic S, Stahl S, Valenzuela T, Vogel M, Werth G, Beier T, Kluge H-J and Quint W 2004 Electronic g factor of hydrogenlike oxygen $^{16}O^{7+}$ *Phys. Rev. Lett.* **92** 093002
[32] Häffner H, Beier T, Djekic S, Hermanspahn N, Kluge H-J, Quint W, Stahl S, Verdú J, Valenzuela T and Werth G 2003 Double Penning trap technique for precise g factor determinations in highly charged ions *Eur. Phys. J.* D **22** 163–82
[33] Wineland D J and Dehmelt H G 1975 Principles of the stored ion calorimeter *J. Appl. Phys.* **46** 919
[34] Jackson J D 2005 *Classical Electrodynamics* (New York: Wiley)
[35] Goldstein H 1980 *Classical Mechanics* (Reading, MA: Addison-Wesley)